

# Indexed-channel estimation under frequency and time-selective fading channels in high-mobility systems

Ali Alqatawneh<sup>1</sup>, Luae Al-Tarawneh<sup>2</sup>, Ziyad Almajali<sup>3</sup>

<sup>1</sup>Computer Engineering and Communication Department, Tafila Technical University, Tafila, Jordan

<sup>2</sup>Communications Engineering Department, Princess Sumaya University for Technology, Amman, Jordan

<sup>3</sup>Electrical Engineering Department, Mu'tah University, Al-Karak, Jordan

## Article Info

### Article history:

Received Jun 10, 2022

Revised Oct 24, 2022

Accepted Dec 2, 2022

### Keywords:

Diversity order

Doppler spread

Energy detection

Index modulation

Pilot symbols

## ABSTRACT

Index modulation (IM) techniques have been employed in different communication systems to improve bandwidth efficiency by carrying additional information bits. In high-mobility communication systems and under both time-selective and frequency-selective fading channels with Doppler spread, channel variations can be tracked by employing pilot-aided channel estimation with minimum mean-squared error estimation. However, inserting pilot symbols among information symbols reduces the system's spectral efficiency in pilot-aided channel estimation schemes. We propose pilot-aided channel estimation with zero-pilot symbols and an energy detection scheme to tackle this issue. Part of the information bit-stream is conveyed by the indices of zero-pilot symbols leading to an increase in the system's spectral efficiency. We used an energy detector at the receiver to detect the transmitted zero-pilot symbols. This paper examines the impacts of diversity order on the zero-pilot symbol detection error probability and the mean-squared of error estimation. The impacts of pilot symbols number and the zero-pilot symbol number on the mean-squared error of the minimum mean-squared error (MMSE) estimator and the system error performance are also investigated in this paper.

This is an open access article under the [CC BY-SA](https://creativecommons.org/licenses/by-sa/4.0/) license.



## Corresponding Author:

Ali Alqatawneh

Computer Engineering and Communication Department, Faculty of Engineering, Tafila Technical University

Tafila, Jordan

Email: ali.qatawneh@ttu.edu.jo

## 1. INTRODUCTION

The availability of high-speed broadband wireless communication services such as online video streaming and gaming, internet of things applications, and multimedia transmission [1] has become necessary in high-speed transport such as aircraft, trains, and unmanned aerial vehicles (UAV) [2]. In high-mobility wireless communication systems, Doppler spread is a critical design parameter that should be considered to maximize the system's performance. High mobility of vehicles, such as high-speed trains (HST), produces a large Doppler spread that can destroy orthogonality among subcarriers in multi-carrier systems leading to intercarrier interference (ICI) [3], [4]. Furthermore, these variations result in channel estimate errors.

It is shown in [5] that the error performance of a communication system with perfectly known channel state information (PNCSI) consistently outperforms an identical system with channel estimation errors, and the performance gap increases with Doppler spread. However, channel variations can provide significant Doppler diversity, leading to performance enhancement [6], [7]. The tradeoff between channel estimation errors and Doppler diversity is investigated in [8]. Results show that a system with imperfect

channel estimation can achieve the same diversity order as a system with PNCISI if the signal-to-noise ratio (SNR) of data and pilot symbols have a linear relationship with each other [9]. The authors of [10] show that at low pilot percentage, the benefits of Doppler diversity might be reduced due to channel estimation errors. If the pilot samples the channel at a rate greater or equal to the Nyquist rate of the time-variant channel, the mean squared of channel estimation at pilot and data symbols is equal [11]. The optimum pilot percentage that maximizes the system spectral efficiency is examined in [12], where the results reveal that the pilot symbols should be assigned more energy with Doppler spread increase. Pilot estimation based on sending pilot symbols is examined in [13] for bad urban, typical urban and rural areas. In adaptive filter-based channel estimation, combining channel estimation and space-time coding can improve channel estimation process [14]. Pilot-assisted channel estimation techniques with least-square (LS) or minimum mean-squared error (MMSE) are widely used [15], [16]. In the Rayleigh and Rician channels, the MMSE estimator outperforms the LS estimator. The MMSE estimator, on the other hand, is more complex than the LS [17]–[19].

Sending pilot symbols among data symbols for channel estimation reduced the spectral efficiency of the wireless system. Spectral efficiency reduction in systems with pilot-assisted based channel estimation schemes can be compensated using index modulation. The primary goal of index modulation is to improve the spectral efficiency of the communication system by sending extra bits using: the indices of the active subcarriers in multi-carrier communication system [20]–[22], indices of Hermite Gaussian pulses [23], indices of pilot positions [24], indices of transmit antennas of multiple input multiple output (MIMO) systems [25], and impedance matching between transmitter and receiver [26]. In [27], the performance of an energy detector for an unknown signal transmitted over fading channels and additive white Gaussian noise (AWGN) is studied. The findings indicate that improving the detection probability considerably improves the detection error performance. Energy detection is commonly used for spectrum sensing in cognitive communication due to its simplicity, and it does not require prior knowledge about the targeted signal [28], [29]; the detection is performed by comparing the energy of the received signal with a predefined threshold.

This paper studies the performance of channel estimations with pilot symbol selection technique in high mobility wireless communications under frequency and time selective fading channels. In the studied system, pilot symbols are inserted among data symbols and then transmitted for channel estimation purposes. Some inserted pilot symbols are zero-pilot symbols; the positions of zero-pilot symbols and their numbers are chosen according to a part of the transmitted data bits. Based on the channel length, extra zeros are added between data and pilot symbols to maintain non-zero pilot symbols from inter-symbol interference. Energy detection is employed at the receiver to detect the zero pilot symbols, and then the transmitted pilot sequence can be determined. From a look-up table, the assigned data bits sent using zero pilot symbols positions can be determined. The detected pilot symbols are then used for channel estimation at pilot and data symbol locations with the help of the MMSE estimator.

This paper also investigates the impact of channel length, number of total pilot symbols, number of zero-pilot symbols, signal-to-noise ratio, and Doppler spread on the mean squared error of channel estimation. The rest of this paper is organized as follows: section 2 presents the system model. Section 3 presents results and discussion, and finally, section 4 concludes the paper.

## 2. RESEARCH METHOD

### 2.1. System model

Consider a wireless communication system that operates on frequency and time-selective fading channels and uses pilot-aided channel estimation with pilot symbol selection technique. In this system, the transmitted bit stream is split into two groups: group  $A$ , with  $p_1$  binary bits, is converted to  $M$ -array phase shift keying (PSK) symbols, and group  $B$ , with  $p_2$  bits, which is transmitted through zero-value primary pilot symbol selection technique. In this technique, a pilot-slot is added after every  $K$ -length  $M$ -array PSK symbols. Each pilot slot contains  $2L - 1$  symbols, where  $L$  is the length of the multipath fading channel. The primary pilot symbol is the middle of the pilot slot, which is selected as 1 or 0 based on bits in the group  $B$ . The rest of the pilot-slot contains  $2L - 1$  zeros or secondary pilots located before and after each primary pilot symbol to prevent the primary pilot symbol from inter-symbol interference (ISI) problems due to frequency and time selective fading channels. The data symbols along with primary and secondary pilot symbols are transmitted as one segment of length  $N + NK$ , where  $N$  is the number of the primary pilot symbols and  $NK$  is the number of data symbols. The relationship between the number of bits in group  $B$  and the number of the primary pilot with zero symbols and the number of inserted primary pilots can be expressed as  $p_2 = \lfloor \log_2(C(N, m)) \rfloor$  with  $C$  being the binomial operation and  $\lfloor \cdot \rfloor$  being the floor function. The number of primary pilot symbols with 0s and their locations are determined based on data bits in group  $B$ .

For each transmitted pilot slot there will be an  $L$  ISI-free received signals. The  $l$ -th received signal of the  $n$ -th transmitted pilot symbol  $x_p(n) \in \{-1, 1, 0\}$  is given as (1):

$$y_p(n) = \sqrt{E_p} h_p(n, l) x_p(n) + w_p(n + l) \quad (1)$$

for

$$n = 0, \dots, (N - 1), l = 0, \dots, L - 1$$

where  $y_p(n)$  is the  $n$ -th received signal at pilot-symbol position,  $h(n, l)$  is the discrete-time impulse response of the transmission channel,  $E_p$  is the energy of the transmitted non-zero pilot symbol, and  $w_p(n + l)$  is the corresponding AWGN with noise power  $N_0$ . We set  $E_p = E_s(2L - 1)$  with  $E_s$  being the energy of each data symbol due to fixed transmission power assumption. Vector format can be used to represent the  $L$  ISI-free received signals from the  $n$ -th transmitted pilot symbol as (2):

$$\begin{bmatrix} y_p(n) \\ y_p(n + 1) \\ \vdots \\ y_p(n + L - 1) \end{bmatrix} = \begin{bmatrix} h_p(n, 0) \\ h_p(n, 1) \\ \vdots \\ h_p(n, L - 1) \end{bmatrix} x_p(n) + \begin{bmatrix} w_p(n) \\ w_p(n + 1) \\ \vdots \\ w_p(n + L - 1) \end{bmatrix} \quad (2)$$

or equivalently (2) can be written as (3):

$$\mathbf{y}_p^n = \sqrt{E_p} \mathbf{h}_p^n x_p(n) + \mathbf{w}_p^n \quad (3)$$

where

$$\mathbf{y}_p^n = \begin{bmatrix} y_p(n) \\ y_p(n + 1) \\ \vdots \\ y_p(n + L - 1) \end{bmatrix}, \mathbf{h}_p^n = \begin{bmatrix} h_p(n, 0) \\ h_p(n, 1) \\ \vdots \\ h_p(n, L - 1) \end{bmatrix}, \mathbf{w}_p^n = \begin{bmatrix} w_p(n) \\ w_p(n + 1) \\ \vdots \\ w_p(n + L - 1) \end{bmatrix}$$

As shown in (3) for every transmitted pilot symbol there would be an  $L$  observed signals at the receiver.

## 2.2. Energy detection of transmitted pilot symbols

In this sub-section, we discuss the application of an energy detector in pilot symbol detection at the receiver side. Depending on the pilot symbol whether zero or non-zero pilot symbol, the observed signals at the receiver for pilot symbols can indicate one of two states that can be modeled as (4) [30]:

$$\mathbf{y}_p^n = \sqrt{E_p} \mathbf{h}_p^n x_p(n) + \mathbf{w}_p^n, \text{ for non zero pilot} \quad (4)$$

$$\mathbf{y}_p^n = \mathbf{w}_p^n, \text{ for zero pilot} \quad (5)$$

So, according to (5), the noise signal is the only signal observed at the receiver when the transmitted pilot is zero-pilot symbol. Energy detection can be employed to determine whether the transmitted pilot is a zero-pilot or a non-zero pilot by computing the energy of the received pilot signals; the computed energy is then compared with a predefined threshold. The energy of the  $n$ -th pilot symbol can be computed as (6):

$$E_n = \frac{1}{\bar{L}} \sum_{l=0}^{\bar{L}-1} |y_p(n + l)|^2 \quad (6)$$

where  $\bar{L}$  is the number of pilot-signal arrival paths that have been taken into consideration when computing the energy of the observed pilot signal;  $\bar{L}$  also represents the diversity order. To collect all benefits from full diversity offered by multipath fading, all observed signal for the  $n$ -th transmitted pilot symbol should be considered in (6), i.e.,  $\bar{L} = L$ . After energy calculation, the transmitted pilot symbol can then be determined as (8):

$$\hat{x}_p(n) = \begin{cases} 1, & \text{if } E_n > N_o \\ 0, & \text{if } E_n \leq N_o \end{cases} \quad (7)$$

where  $\lambda=N_o$  is considered as the detection threshold. The detected pilot symbols can be expressed in vector format as  $\hat{\mathbf{x}}_p(n) = [\hat{x}_p(1), \hat{x}_p(2), \dots, \hat{x}_p(N)]$ . After detecting all the transmitted pilot symbols, the transmitted bits sent over the indices of zero-pilot symbols can then be specified using a predetermined lookup table.

**2.3. Pilot-based channel estimation**

After detecting the pilot symbols, the detected pilot symbols are used for channel estimation. This sub-section presents channel estimation based on the detected pilot symbols. After detecting all pilot symbols, the observed signals from all pilot symbols can be approximately expressed in vector format as (8):

$$\hat{\mathbf{y}}_p = \sqrt{E_p} \mathbf{h}_p \hat{\mathbf{X}}_p + \mathbf{w}_p \tag{8}$$

where

$$\mathbf{h}_p = \begin{bmatrix} \mathbf{h}_p^0 \\ \mathbf{h}_p^1 \\ \vdots \\ \mathbf{h}_p^{N_p-1} \end{bmatrix}, \hat{\mathbf{X}}_p = \text{diag}(\hat{\mathbf{x}}_p \otimes \mathbf{1}_{L \times 1}), \text{and } \mathbf{w}_p = \begin{bmatrix} \mathbf{w}_p^0 \\ \mathbf{w}_p^1 \\ \vdots \\ \mathbf{w}_p^{N_p-1} \end{bmatrix}$$

with  $\otimes$  being the Kronecker tensor product. The channel coefficients at pilot positions can be estimated as  $\hat{\mathbf{h}}_p = \mathbf{D}_p^H \mathbf{y}_p$ , where  $\mathbf{D}_p$  denotes the channel estimation matrix. By minimizing the mean-squared error (MSE) between the estimated channel coefficients and the true ones, and based on the orthogonal principle  $E[(\hat{\mathbf{h}}_p - \mathbf{h}_p) \hat{\mathbf{y}}_p^H]$ , with  $E$  being the mathematical expectation. The estimation channel matrix can be obtained as [15]:

$$E[(\hat{\mathbf{h}}_p \mathbf{y}_p^H - \mathbf{h}_p \mathbf{y}_p^H)] = E[(\mathbf{D}_p^H \mathbf{y}_p \mathbf{y}_p^H - \mathbf{h}_p \mathbf{y}_p^H)] = 0 \tag{9}$$

where

$$E[\mathbf{D}_p^H \mathbf{y}_p \mathbf{y}_p^H] = \mathbf{D}_p^H (E_p \hat{\mathbf{X}}_p \mathbf{D}_{pp} \hat{\mathbf{X}}_p^H + N_o \mathbf{I}_{LN_p})^{-1} \tag{10}$$

and

$$E[\mathbf{h}_p \mathbf{y}_p^H] = \sqrt{E_p} E[\mathbf{h}_p (\mathbf{h}_p^H \hat{\mathbf{X}}_p^H + \mathbf{w}_p^H)] = \sqrt{E_p} \mathbf{D}_{pp} \hat{\mathbf{X}}_p^H \tag{11}$$

where  $\mathbf{D}_{pp} = E[\mathbf{h}_p \mathbf{h}_p^H]$ . From (9)-(11) we can find the minimum MSE (MMSE) estimation matrix as (12):

$$\mathbf{D}_p = \sqrt{E_p} (E_p \hat{\mathbf{X}}_p \mathbf{D}_{pp} \hat{\mathbf{X}}_p^H + N_o \mathbf{I}_{LN_p})^{-1} \hat{\mathbf{X}}_p \mathbf{D}_{pp} \tag{12}$$

Following the procedure above, the pilot symbols at data positions can be estimated as  $\hat{\mathbf{h}}_d = \mathbf{D}_d \hat{\mathbf{h}}_p$ , where  $\mathbf{D}_d$  represents the estimation matrix. By minimizing the mean-squared error between the estimated channel coefficient and the real ones, and based on the orthogonal principle, the estimation channel matrix can be obtained as  $E[(\hat{\mathbf{h}}_d - \mathbf{h}_d) \hat{\mathbf{h}}_p^H] = E[(\hat{\mathbf{h}}_d \hat{\mathbf{h}}_p^H - \mathbf{h}_d \hat{\mathbf{h}}_p^H)] = E[\mathbf{D}_d \hat{\mathbf{h}}_p \hat{\mathbf{h}}_p^H - \mathbf{h}_d (\mathbf{D}_d \mathbf{y}_p)^H]$ , from which we can find  $\mathbf{D}_d$  as (13).

$$\mathbf{D}_d = \sqrt{E_p} \mathbf{D}_{dp} \hat{\mathbf{X}}_p^H \mathbf{D}_p \left( \mathbf{D}_p^H (E_p \hat{\mathbf{X}}_p \mathbf{D}_{pp} \hat{\mathbf{X}}_p^H + N_o \mathbf{I}_{LN_p}) \mathbf{D}_p \right)^{-1} \tag{13}$$

where  $\mathbf{D}_{dp} = E[\mathbf{h}_d \mathbf{h}_p^H]$ . The channel coefficients at data-symbols locations are then estimated as (14) [15]:

$$\hat{\mathbf{h}}_d = \sqrt{E_p} \mathbf{D}_{dp} \hat{\mathbf{X}}_p^H (E_p \hat{\mathbf{X}}_p \mathbf{D}_{pp} \hat{\mathbf{X}}_p^H + N_o \mathbf{I}_{LN_p})^{-1} \hat{\mathbf{y}}_p \tag{14}$$

**2.4. Channel estimation mean-squared error**

To calculate the MSE of channel estimation associated with pilot symbols, let  $\mathbf{e}_p = \hat{\mathbf{h}}_p - \mathbf{h}_p$ , then the auto-correlation matrix of channel estimation error,  $\mathbf{P}_e$ , can be defined as  $\mathbf{P}_e = E[\mathbf{e}_p \mathbf{e}_p^H] = E[(\hat{\mathbf{h}}_p - \mathbf{h}_p)(\hat{\mathbf{h}}_p - \mathbf{h}_p)^H]$  and can be obtained as (15).

$$\mathbf{P}_e = \mathbf{D}_{pp} - \mathbf{D}_{pp} \widehat{\mathbf{X}}_p^H (E_p \widehat{\mathbf{X}}_p \mathbf{D}_{pp} \widehat{\mathbf{X}}_p^H + \frac{N_0}{E_s(2L-1)} \mathbf{I}_{LN_p})^{-1} \widehat{\mathbf{X}}_p \mathbf{D}_{pp}^H \quad (15)$$

Furthermore, the MSE of channel estimation of channel coefficients at the data positions can be obtained as  $\sigma_p = \frac{1}{KN} \sum_{k=1}^{KN} \phi_k$ , where  $\phi_k$  is the eigenvalues of the matrix  $\mathbf{P}_e$ . Likewise, to calculate the MSE estimation of channel coefficients at data symbols positions, let  $\mathbf{e}_d = \widehat{\mathbf{h}}_d - \mathbf{h}_d$ , then the auto-correlation noise matrix  $\Psi_e = E[\mathbf{e}_d \mathbf{e}_d^H]$  can be found as

$$\Psi_e = \mathbf{D}_{dd} - \mathbf{D}_{dp} \widehat{\mathbf{X}}_p^H (E_p \widehat{\mathbf{X}}_p \mathbf{D}_{pp} \widehat{\mathbf{X}}_p^H + \frac{N_0}{E_s(2L-1)} \mathbf{I}_{LN})^{-1} \widehat{\mathbf{X}}_p \mathbf{D}_{dp}^H \quad (16)$$

The MSE of channel estimation of channel coefficients at the data positions can be calculated as

$$\sigma_d = \frac{1}{KN} \sum_{k=1}^{KN} \lambda_k,$$

where  $\lambda_k$  is the eigenvalues of the matrix  $\Psi_e$  [31].

### 3. RESULTS AND DISCUSSION

In this section, we present the performance and the mean-squared error of channel estimation for a system with an energy detection-based pilot channel estimation operating under frequency and time-selective fading channels. In the simulation, we consider a multipath fading model with equal power taps. Also, we assume that the data symbol energy is  $E_s = 1$  and the data slot length is  $K = 1$ . In Figure 1, the simulated primary-pilot symbol energy detection probability of error ( $PE$ ) is shown for three different levels of diversities under a channel of length  $L = 3$ . The curves were obtained for systems with  $N = 8$ ,  $m = 2$ , and  $f_D T_s = 0.003$ . As expected, the best performance occurs at the full diversity with diversity order equals  $\bar{L} = 3$ . As an illustration, the detection probability of error at  $E_b/N_0 = 20$  dB is  $1.14 \times 10^{-2}$  at diversity order  $\bar{L} = 1$ , while, the detection probability of error reduces to  $2.906 \times 10^{-4}$ , and  $5 \times 10^{-6}$  at  $\bar{L} = 2$  and  $\bar{L} = 3$ , respectively.

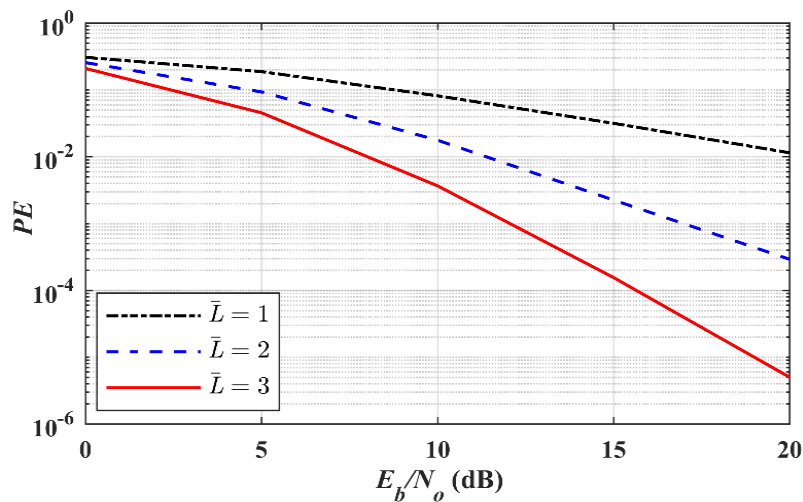


Figure 1. Presenting the simulated primary pilot-symbols detection error probability as a function of the signal-to-noise ratio,  $E_b/N_0$ , under different diversity orders

The detection error probabilities for the transmitted primary-pilot symbols and bits transmitted through a primary-pilot symbol selection under different channel lengths are presented in Figure 2. Simulations were performed under the full-diversity assumption. Furthermore, all error probability curves were obtained for systems with  $N = 8$ ,  $m = 3$ ,  $f_D T_s = 0.003$ , and  $T_s = 3.69 \mu s$ . According to Figure 2, the detection error probabilities for both primary-pilot symbols and bits transmitted via zero-primary-pilot symbol selection show improvement with channel length increase. This improvement is due to an enhancement in a multipath diversity gain caused by the rise in the channel length.

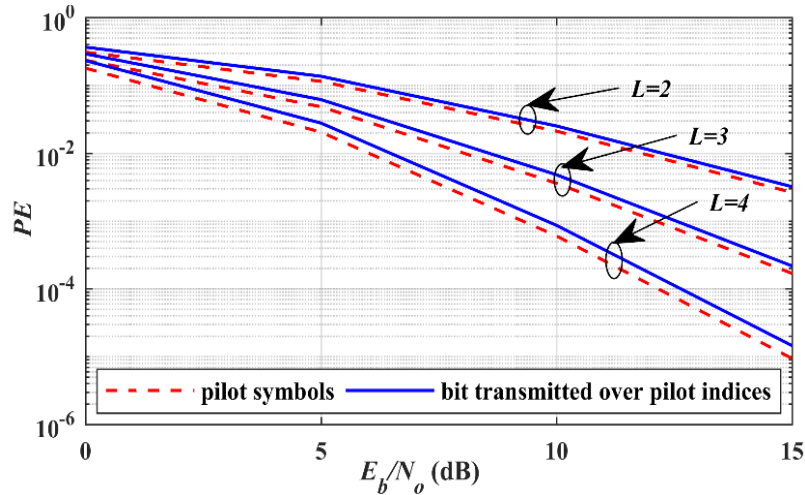


Figure 2. Illustrating the probability of error of the primary-pilot symbol detection and the probability of error for bits transmitted via indices of zero-primary pilot symbols as a function of signal-to-noise ratio,  $E_b/N_o$ , under different channel lengths

Figure 3 shows plots the mean-squared error (MSE) of channel estimation at pilot-symbol positions as a function of  $E_b/N_o$  and under different channel lengths. We assume  $N = 16, f_D T_s = 0.002, m = 2$  and full diversity for all systems. Perfect matching between simulation and analytical results can be easily seen from the figure. As expected and due to the enhancement in multipath-diversity gain, the mean-squared error of channel estimation for the proposed system decreases as channel length increases. As an example, at  $E_b/N_o=10$  dB, the MSE is  $2.3 \times 10^{-3}$  when  $L=4$ ; however, it increases to  $3 \times 10^{-3}$ , and  $4.5 \times 10^{-3}$  when  $L=3$ , and  $L=2$ , respectively.

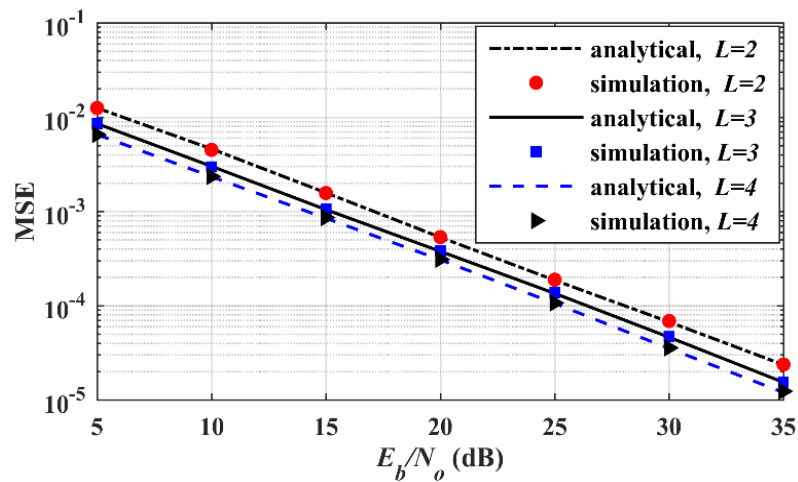


Figure 3. Presenting the MSE of channel estimation at pilot positions as a function of signal-to-noise ratio,  $E_b/N_o$ , for various values of  $L$

In Figure 4, we plot the simulated and the numerical mean-squared error of channel estimation at pilot and data symbol locations. The mean-squared error curves were plotted as a function of  $E_b/N_o$  under various numbers of pilot symbols. The system parameters used in simulations are  $m=2, f_D T_s = 0.002, L = 2$ , and diversity order  $\bar{L} = 2$ . We can see an excellent agreement between simulation and numerical results. As predicted, at a given number of zero-primary pilot symbols,  $m$ , a larger value of primary pilot symbols,  $N$ , can reduce the mean-squared error of channel estimation. Thus, a longer transmitted sequence can provide better channel estimation.

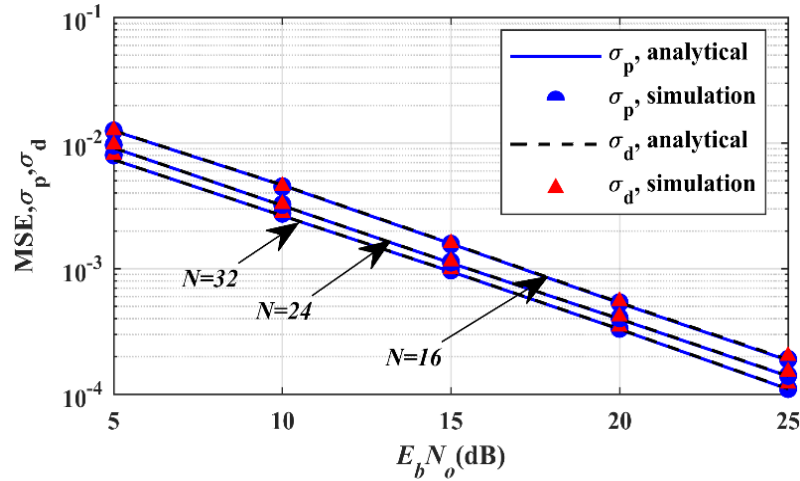


Figure 4. plotting the MSE of channel coefficient estimation as a function of signal-to-noise ratio,  $E_b/N_0$ , and under different pilot numbers,  $N$

In Figure 5, we compare the simulated MSE of the proposed system with the simulated MSE of a system with a conventional channel estimation scheme at which  $m = 0$ . In the figure, we plot the MSEs as a function of  $E_b/N_0$  under different numbers of zero-primary pilot symbols,  $m$ . The systems parameters are set as  $T_s = 3.69 \mu s$ ,  $f_p T_s = 0.001$ , and  $L = 2$  with full diversity order. As expected, the MSE is a decreasing function of the zero-primary pilot symbol percentage  $m/N$ , rising this percentage leads to channel estimation error reduction. Figure 5 shows that, at  $N = 16$  increasing  $m$  from 2 to 5 leads to an increase in MSE over its counterpart in the classical system. However, the MSE difference between the proposed and the conventional systems becomes very small when the number of primary pilots increases to  $N = 48$ . For example, at  $N = 48$  and  $m = 0$ , an MSE of  $10^{-4}$  can be reached at a signal-to-noise ratio of 23.25 dB; however, we need extra 0.75 dB to reach the same MSE value when  $m = 5$ . On the other hand, at  $N = 16$ , the MSE of  $10^{-4}$  is reached at a signal-to-noise ratio of 26.5 dB when  $m = 0$ , the required signal-to-noise ratio increases to 28.5 dB to reach the same MSE value when  $m = 5$ .

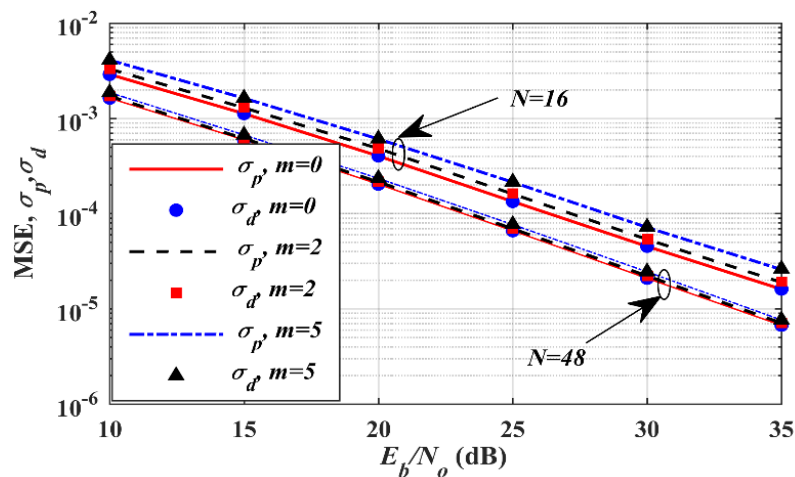


Figure 5. Presenting the MSE of channel estimation for the proposed system as a function of signal-to-noise ratio,  $E_b/N_0$  and under different system configurations

In Figure 6, the MSE of the proposed system is plotted as a function of the number of zero-pilot symbols,  $m$ , under different values of inserted pilot symbols  $N$ . The system parameters are set as  $E_b/N_0 = 15$  dB,  $L = 2$ ,  $T_s = 66.7 \mu s$ ,  $f_D T_s = 0.001$ , and full diversity. From Figure 6, we can see that increasing the number of zero-pilot symbols leads to an increase in the MSE of the proposed system. This

increase widens the channel estimation error gap between the proposed system and an equivalent system with the classical channel estimation at which  $m=0$ . However, this gap can be reduced by increasing the number of pilot symbols. For example, at  $m=6$ , the MSE percentage difference between the two systems is 55.45% at  $N = 16$ ; fortunately, it becomes 14.45% when  $N = 48$ .

Figure 7 shows the MSE of channel estimation for the proposed system at both pilot and data symbols positions versus  $f_D T_s$  for different values of  $E_b/N_o$ . We set the simulation parameters as  $N = 32, m = 2, L = 2, T_s = 3.69\mu s$ , and full diversity order. From the figure we note that there are agreements between simulated and analytical results. Furthermore, the figure shows that the mean-squared error for channel estimations increases with Doppler diversity rise. However, at the same value of Doppler spread  $f_D$ , increasing  $E_b/N_o$  leads to a reduction in the mean-squared error of channel estimation.

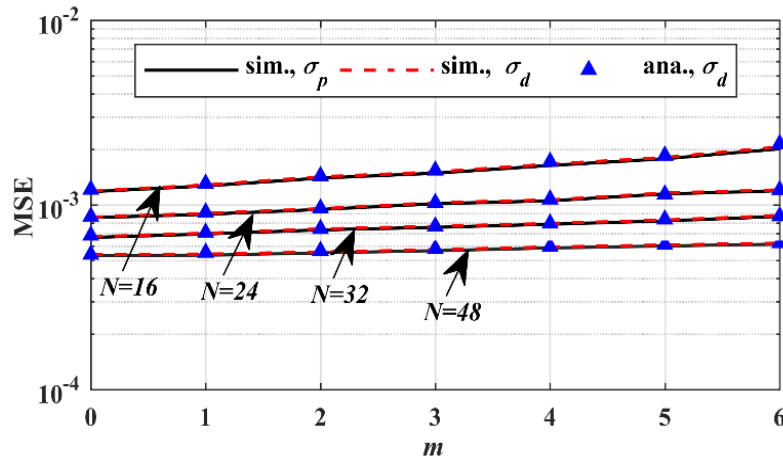


Figure 6. Illustrating the MSE of channel estimation at pilot and data positions as a function of the number of zero-primary pilot symbols  $m$

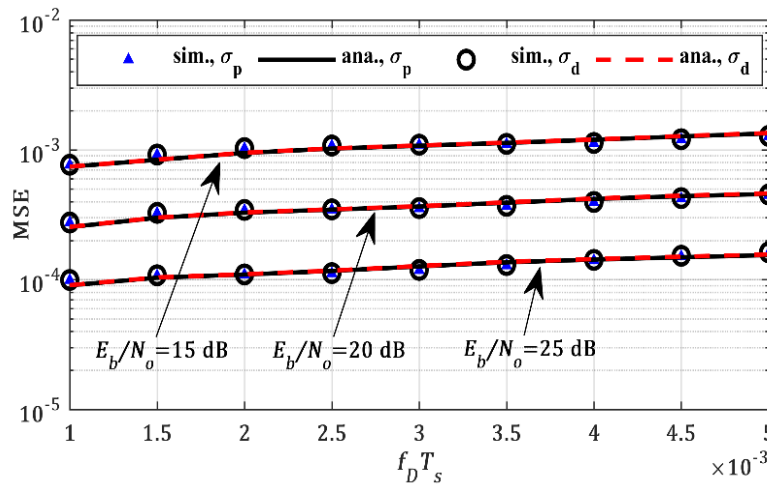


Figure 7. Presenting the MSE of channel estimation at both pilot and data positions versus  $f_D T_s$ . The curves obtained at different values of signal-to-noise ratio,  $E_b/N_o$

Finally, Figure 8 presents the MSE of channel estimation at pilot-symbol locations for the proposed system as a function of  $f_D T_s$ . The Results are obtained under different values of  $E_b/N_o$ , and number of primary-pilot symbols  $N$ . The system configurations are set as  $m = 2, L = 2$ , and full diversity order. As expected, at fixed Doppler spread and zero-primary pilot symbols, the channel estimation errors can be reduced either by increasing the number of pilot symbols or by increasing the signal-to-noise ratio  $E_b/N_o$ . For example, at  $f_D T_s = 0.005$  the value of the MSE is  $4.4 \times 10^{-3}$  when  $E_b/N_o$  equals to 10 dB, while at the



same value of  $f_D T_s$  the MSE value reduces to  $1.57 \times 10^{-4}$  when  $E_b/N_0$  equals to 25 dB. Moreover, at  $f_D T_s = 0.004$  and  $E_b/N_0 = 25$  dB the values of MSE are  $4.6 \times 10^{-3}$ ,  $2.45 \times 10^{-4}$ , and  $1.44 \times 10^{-4}$  when  $N = 8, 16$  and  $32$ , respectively.

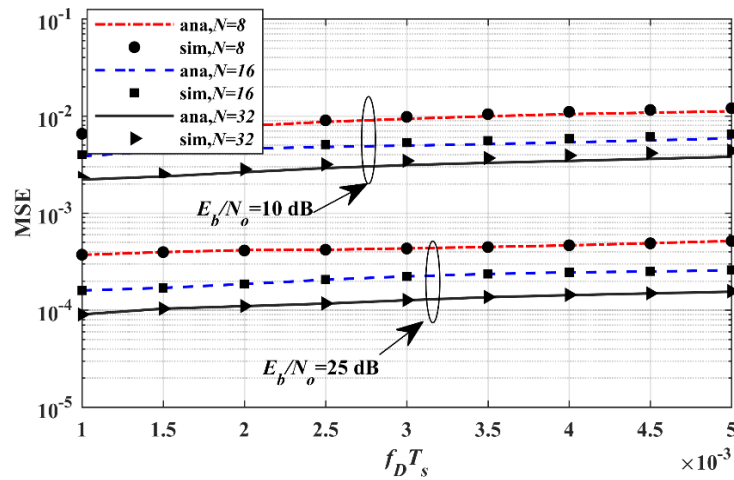


Figure 8. Presenting the MSE of channel estimation at both pilot and data positions versus  $f_D T_s$ . The curves obtained at different pilot numbers

#### 4. CONCLUSION

This paper presents a pilot-aided channel estimation system with zero-primary pilot symbol selection. In this system, we set some selected primary pilot symbols to zero. The locations of these zero-pilot symbols are employed to transmit extra data bits over frequency and time-selective fading channels. Energy detection has been used at the receiver to detect the transmitted zero-pilot symbols. In this paper, we examine the impacts of diversity order on both the zero-pilot symbol detection error probability and the mean squared error of channel estimation. We have also studied channel length's effect on the collected diversity and the overall system performance. Our results showed that increasing the number of zero-primary pilot symbols can improve system throughput and increase channel estimation errors. It turns out that, at a fixed number of zero-primary pilot symbols, increasing the number of primary pilot symbols inserted among the data symbol can significantly reduce channel estimation errors.





#### REFERENCES

- [1] A. Rafay, S. M. Idrus, K. M. Yusof, and S. H. Mohammad, "A survey on advanced transmission technologies for high bandwidth and good signal quality for high-speed railways," *Indonesian Journal of Electrical Engineering and Computer Science (IJECS)*, vol. 23, no. 1, pp. 293–301, Jul. 2021, doi: 10.11591/ijeecs.v23.i1.pp293-301.
- [2] V. A. Aalo, P. S. Bithas, and G. P. Efthymoglou, "On the impact of user mobility on the performance of wireless receivers," *IEEE Access*, vol. 8, pp. 197300–197311, 2020, doi: 10.1109/ACCESS.2020.3034450.
- [3] H. Zhang, W. Li, and Y. Xu, "EM-based channel estimation with index modulation for high speed train communication," in *2019 International Conference on Communications, Information System and Computer Engineering (CISCE)*, Jul. 2019, pp. 390–394, doi: 10.1109/CISCE.2019.00092.
- [4] Z. Sheng, H. D. Tuan, H. H. Nguyen, and Y. Fang, "Pilot optimization for estimation of high-mobility OFDM channels," *IEEE Transactions on Vehicular Technology*, vol. 66, no. 10, pp. 8795–8806, Oct. 2017, doi: 10.1109/TVT.2017.2694821.
- [5] W. Zhou, J. Wu, and P. Fan, "On the maximum Doppler diversity of high mobility systems with imperfect channel state information," in *2015 IEEE International Conference on Communications (ICC)*, Jun. 2015, pp. 4431–4436, doi: 10.1109/ICC.2015.7249020.
- [6] X. Hou, J. Ling, and D. Wang, "Performance of high-mobility MIMO communications with Doppler diversity," *IEEE Access*, vol. 8, pp. 31574–31585, 2020, doi: 10.1109/ACCESS.2020.2973268.
- [7] W. Zhou, J. Wu, and P. Fan, "High mobility wireless communications with doppler diversity: fundamental performance limits," *IEEE Transactions on Wireless Communications*, vol. 14, no. 12, pp. 6981–6992, Dec. 2015, doi: 10.1109/TWC.2015.2463276.
- [8] M. A. Mahamadu, J. Wu, Z. Ma, W. Zhou, Y. Tang, and P. Fan, "Fundamental tradeoff between doppler diversity and channel estimation errors in SIMO high mobility communication systems," *IEEE Access*, vol. 6, pp. 21867–21878, 2018, doi: 10.1109/ACCESS.2018.2826438.
- [9] M. A. Mahamadu, J. Wu, Z. Ma, W. Zhou, and P. Fan, "Maximum diversity order of SIMO high mobility systems with imperfect channel state information," in *2017 IEEE 17th International Conference on Communication Technology (ICCT)*, Oct. 2017, pp. 212–217, doi: 10.1109/ICCT.2017.8359633.
- [10] W. Zhou, J. Wu, and P. Fan, "Spectral efficient doppler diversity transmissions in high mobility systems with channel estimation errors," in *2015 IEEE 81st Vehicular Technology Conference (VTC Spring)*, May 2015, vol. 2015, no. 1, pp. 1–6, doi:




- 10.1109/VTCSpring.2015.7146098.
- [11] N. Sun and J. X. Wu, "Maximizing spectral efficiency with imperfect channel information in high mobility systems," in *2013 IEEE Global Communications Conference (GLOBECOM)*, Dec. 2013, pp. 3359–3364, doi: 10.1109/GLOCOM.2013.6831591.
  - [12] N. Sun, J. Wu, and P. Fan, "Optimum designs of high mobility wireless systems with channel estimation errors," *IET Communications*, vol. 9, no. 13, pp. 1677–1682, Sep. 2015, doi: 10.1049/iet-com.2014.0952.
  - [13] H. A.-J. Al-Asady, H. F. Fakhruddin, and M. Q. Alsudani, "Channel estimation of OFDM in C-band communication systems under different distribution conditions," *Indonesian Journal of Electrical Engineering and Computer Science (IJECS)*, vol. 23, no. 3, pp. 1778–1782, Sep. 2021, doi: 10.11591/ijeecs.v23.i3.pp1778-1782.
  - [14] S. Pyla, K. Padma Raju, and N. B. Subrahmanyam, "Performance analysis of adaptive filter channel estimated MIMO OFDM communication system," *International Journal of Electrical and Computer Engineering (IJECE)*, vol. 8, no. 5, pp. 3829–3838, Oct. 2018, doi: 10.11591/ijece.v8i5.pp3829-3838.
  - [15] A. Alqatawneh and L. Tarawneh, "OFDM system with half-symbol-spaced receiver and channel acquisition error over multipath fading channels," *Jordan Journal of Electrical Engineering*, vol. 7, no. 2, 2021, doi: 10.5455/jjee.204-1613432117.
  - [16] J.-W. Choi and Y.-H. Lee, "Optimum pilot pattern for channel estimation in OFDM systems," *IEEE Transactions on Wireless Communications*, vol. 4, no. 5, pp. 2083–2088, Sep. 2005, doi: 10.1109/TWC.2005.853891.
  - [17] M. B. Sutar and V. S. Patil, "LS and MMSE estimation with different fading channels for OFDM system," in *2017 International Conference of Electronics, Communication and Aerospace Technology (ICECA)*, Apr. 2017, pp. 740–745, doi: 10.1109/ICECA.2017.8203641.
  - [18] M. K. Abboud and B. M. Sabbar, "Performance evaluation of high mobility OFDM channel estimation techniques," *International Journal of Electrical and Computer Engineering (IJECE)*, vol. 10, no. 3, pp. 2562–2568, Jun. 2020, doi: 10.11591/ijece.v10i3.pp2562-2568.
  - [19] J. A. Sam and A. K. Nair, "Analysis and implementation of channel estimation in OFDM system using pilot symbols," in *2016 International Conference on Control, Instrumentation, Communication and Computational Technologies (ICCICCT)*, Dec. 2016, pp. 725–728, doi: 10.1109/ICCICCT.2016.7988047.
  - [20] J. Li, S. Dang, M. Wen, X.-Q. Jiang, Y. Peng, and H. Hai, "Layered orthogonal frequency division multiplexing with index modulation," *IEEE Systems Journal*, vol. 13, no. 4, pp. 3793–3802, Dec. 2019, doi: 10.1109/JSYST.2019.2918068.
  - [21] P. Wei, C. Zhou, Y. Xiao, and S. Q. Li, "GFDM with interleaved subcarrier-index modulation," *Dianzi Keji Daxue Xuebao/Journal of the University of Electronic Science and Technology of China*, vol. 46, no. 3, pp. 516–521, 2017, doi: 10.3969/j.issn.1001-0548.2017.03.007.
  - [22] S. Althunibat, R. Mesleh, and E. Basar, "Differential subcarrier index modulation," *IEEE Transactions on Vehicular Technology*, vol. 67, no. 8, pp. 7429–7436, Aug. 2018, doi: 10.1109/TVT.2018.2837691.
  - [23] S. Aldirmaz-Colak, E. Aydin, Y. Celik, Y. Acar, and E. Basar, "Pulse index modulation," *IEEE Communications Letters*, vol. 25, no. 7, pp. 2309–2313, Jul. 2021, doi: 10.1109/LCOMM.2021.3073753.
  - [24] Q. Li, M. Wen, Y. Zhang, J. Li, F. Chen, and F. Ji, "Pilot insertion with index modulation for OFDM-based vehicular communications," in *2018 IEEE Global Conference on Signal and Information Processing (GlobalSIP)*, Nov. 2018, pp. 1204–1208, doi: 10.1109/GlobalSIP.2018.8646384.
  - [25] E. Basar, M. Wen, R. Mesleh, M. Di Renzo, Y. Xiao, and H. Haas, "Index modulation techniques for next-generation wireless networks," *IEEE Access*, vol. 5, pp. 16693–16746, 2017, doi: 10.1109/ACCESS.2017.2737528.
  - [26] H. Y. LEE and S. Y. Shin, "A novel index modulation scheme with impedance matching," *Indonesian Journal of Electrical Engineering and Computer Science (IJECS)*, vol. 14, no. 3, pp. 1203–1209, Jun. 2019, doi: 10.11591/ijeecs.v14.i3.pp1203-1209.
  - [27] R. Agarwal, N. Srivastava, and H. Katiyar, "On the energy detection of unknown signals over fading channel for different diversity combining techniques," in *Proceedings of the International Conference on Industrial Engineering and Operations Management*, 2016, no. 1.
  - [28] S. Rodriguez-Parera, V. Ramon, A. Bourdoux, F. Horlin, and R. Lauwereins, "Spectrum sensing over SIMO multi-path fading channels based on energy detection," in *IEEE GLOBECOM 2008 - 2008 IEEE Global Telecommunications Conference*, 2008, pp. 1–6, doi: 10.1109/GLOCOM.2008.ECP.571.
  - [29] G. M. Salama and S. A. Taha, "Cooperative spectrum sensing and hard decision rules for cognitive radio network," in *2020 3<sup>rd</sup> International Conference on Computer Applications and Information Security (ICCAIS)*, Mar. 2020, pp. 1–6, doi: 10.1109/ICCAIS48893.2020.9096740.
  - [30] S. Atapattu, C. Tellambura, and H. Jiang, "Performance of an energy detector over channels with both multipath fading and shadowing," *IEEE Transactions on Wireless Communications*, vol. 9, no. 12, pp. 3662–3670, Dec. 2010, doi: 10.1109/TWC.2010.100110.091042.
  - [31] S. M. Blinder, "Guide to essential math: a review for physics, chemistry and engineering students," *Choice Reviews Online*, vol. 46, no. 7, pp. 46-3902-46-3902, Mar. 2009, doi: 10.5860/CHOICE.46-3902.

## BIOGRAPHIES OF AUTHORS






**Ali Alqatawneh**     is an Assistant Professor at Computer Engineering and Communication Department at Tafila Technical University, Jordan. He received a B.Sc. degree in communication engineering from Mu'tah University, Jordan, an M.Sc. degree in communication engineering from Mu'tah University, and a Ph.D. degree in Electrical Engineering with a specialization in wireless communication from the University of Arkansas, USA. His research experience covers various topics in wireless communications, such as multicarrier multiple access techniques, channel estimation techniques, high mobility wireless communications, cognitive radio networks, and orthogonal frequency division multiplexing with index modulation. He can be contacted at email: ali.qatawneh@ttu.edu.jo.



**Luae Al-Tarawneh**    received his Ph.D. degree in electrical and computer engineering from Southern Illinois University (SIU), Carbondale, Illinois in 2016, USA, M.Sc. degree in communications engineering from the University of Jordan, Amman, Jordan in 2008, and B.Sc. degree in communications engineering from Mu'tah University, Al-Karak, in 1999. Dr. Al-Tarawneh has been with the department of communications engineering at Princess Sumaya University for Technology (PSUT) since January 2019. He currently serves as an assistant professor of communications engineering at PSUT. Dr. Al-Tarawneh's current research interests are in optical communication networks, wireless communications and related fields. He can be contacted at email: l.altarawneh@psut.edu.jo.



**Ziyad Almajali**    is an Assistant Professor at Electrical Engineering Department, Mu'tah University, Al-Karak, Jordan. since 2015. Received his Ph.D. degree in electrical and electronic engineering from Liverpool University in 2016, UK, M.Sc. degree in electrical and computer engineering from New York Institute of Technology, Amman, Jordan in 2004, and B.Sc. degree in electrical engineering from Mu'tah University, Al-Karak, in 1997. His research interests are in Smart Grids challenges in Electrical Power Systems and its related fields. He can be contacted at email: ziyad@mutah.edu.jo.